PREPARATION AND TESTING OF CORROSION- AND SPALLATION-RESISTANT COATINGS

Annual Topical Report

Reporting Period Start Date: October 1, 2014
Reporting Period End Date: September 30, 2015

Project Reporting Period: October 1, 2011 – June 30, 2016

Principal Author: John P. Hurley

Report Issue Date: October 2015
Cooperative Agreement No. DE-FE0007325

Submitting Organization:
Energy & Environmental Research Center
University of North Dakota
15 North 23rd Street, Stop 9018
Grand Forks, ND 58202-9018

John P. Hurley, Project Manager

October 2015

EERC DISCLAIMER

LEGAL NOTICE This research report was prepared by the Energy & Environmental Research Center (EERC), an agency of the University of North Dakota, as an account of work sponsored by the U.S. Department of Energy (DOE) National Energy Technology Laboratory. Because of the research nature of the work performed, neither the EERC nor any of its employees makes any warranty, express or implied, or assumes any legal liability or responsibility for the accuracy, completeness, or usefulness of any information, apparatus, product, or process disclosed or represents that its use would not infringe privately owned rights. Reference herein to any specific commercial product, process, or service by trade name, trademark, manufacturer, or otherwise does not necessarily constitute or imply its endorsement or recommendation by the EERC.

ACKNOWLEDGMENT

This material is based upon work supported by DOE under Award No. DE-FE0007325.

DOE DISCLAIMER

This report was prepared as an account of work sponsored by an agency of the United States Government. Neither the United States Government, nor any agency thereof, nor any of their employees, makes any warranty, express or implied, or assumes any legal liability or responsibility for the accuracy, completeness, or usefulness of any information, apparatus, product, or process disclosed, or represents that its use would not infringe privately owned rights. Reference herein to any specific commercial product, process, or service by trade name, trademark, manufacturer, or otherwise does not necessarily constitute or imply its endorsement, recommendation, or favoring by the United States Government or any agency thereof. The views and opinions of authors expressed herein do not necessarily state or reflect those of the United States Government or any agency thereof.

PREPARATION AND TESTING OF CORROSION- AND SPALLATION-RESISTANT COATINGS

ABSTRACT

This Energy & Environmental Research Center (EERC) project is designed to determine if plating APMT®, a specific highly oxidation-resistant oxide dispersion-strengthened FeCrAl alloy made by Kanthal, onto nickel-based superalloy turbine parts is a viable method for substantially improving the lifetimes and maximum use temperatures of the parts. The method for joining the APMT plate to the superalloys is called evaporative metal bonding and involves placing a thin foil of zinc between the plate and the superalloy, clamping them together, and heating in an atmosphere-controlled furnace. Upon heating, the zinc melts and dissolves the oxide skins of the alloys at the bond line, allowing the two alloys to diffuse into each other. The zinc then diffuses through the alloys and evaporates from their surfaces.

During this annual reporting period, the finite element model was completed and used to design clamping jigs to hold the APMT plate to the larger blocks of superalloys during the bonding process. The clamping system was machined from titanium–zirconium–molybdenum and used to bond the APMT plate to the superalloy blocks. The bond between the APMT plate was weak for one of each of the superalloy blocks. We believe that this occurred because enough oxidation had occurred on the surface of the parts as a result of a 1-month time period between sandblasting to prepare the parts and the actual bonding process. The other blocks were, therefore, bonded within 1 day of preparing the parts for bonding, and their joints appear strong. Scanning electron microscopy analyses of representative joints showed that no zinc remained in the alloys after bonding. Also, phases rich in hafnium and tantalum had precipitated near the bond line in the APMT. Iron from the APMT had diffused into the superalloys during bonding, more extensively in the CM247LC than in the Rene 80. Nickel from the superalloys had diffused into the APMT, again more extensively in the joint with the CM247LC than with the Rene 80. One-inch-diameter buttons were machined from each of the bonded blocks and sent to Siemens for standard oxidation, spallation, and corrosion testing, which should be complete in the spring of 2016.

TABLE OF CONTENTS

LIST OF FIGURES

LIST OF TABLES

NOMENCLATURE

APMT®	oxide dispersion-strengthened FeCrAl alloy made by Kanthal
CM247LC	alumina scale-forming nickel-based superalloy
EDM	electrodishcharge-machined
EDS	energy-dispersive spectroscopy
EERC	Energy & Environmental Research Center
EMB	evaporative metal bonding
Rene® 80	alumina scale-forming nickel-based superalloy
SEM	scanning electron microscopy
TBC	thermal barrier coating
TZM	titanium–zirconium–molybdenum
UTSR	University Turbine Systems Research

PREPARATION AND TESTING OF CORROSION- AND SPALLATION-RESISTANT COATINGS

EXECUTIVE SUMMARY

This Energy & Environmental Research Center (EERC) project was designed to determine if plating APMT®, a specific highly oxidation-resistant oxide dispersion-strengthened FeCrAl alloy made by Kanthal, onto nickel-based superalloy turbine parts is a viable method for substantially improving the lifetimes and maximum use temperatures of the parts, both those with thermal barrier coatings and those without. The superalloys being investigated for protection are CM247LC and Rene® 80. Both are alumina-scale-forming alloys. The method for bonding the APMT plate to the superalloys is called evaporative metal bonding, which involves placing a thin foil of zinc between the plate and the superalloy, clamping them together, and heating in an atmosphere-controlled furnace. Upon heating, the zinc melts and dissolves the oxide skins of the alloys at the bond line, allowing the two alloys to diffuse into each other. The zinc then diffuses through the alloys and evaporates from their surfaces.

If successful, the information developed will help move the protection process closer to demonstration testing. In addition, the team will characterize the microcontaminants in combusted higher-hydrogen-content gas. This information will be used to best simulate actual corrosion conditions in a turbine system and can also be used by other researchers studying deposition and gas flow in turbines.

During this annual reporting period, the finite element model was completed and used to design clamping jigs to hold the APMT plate to the larger blocks of superalloys during the bonding process. The clamping system was machined from titanium–zirconium–molybdenum and used to bond the APMT plate to the superalloy blocks. The bond between the APMT plate was weak for one of each of the superalloy blocks. We believe that this occurred because enough oxidation had occurred on the surface of the parts as a result of a 1-month time period between sandblasting to prepare the parts and the actual bonding process. The other blocks were, therefore, bonded within 1 day of preparing the parts for bonding, and their joints appear strong. Scanning electron microscopy analyses of representative joints showed that no zinc remained in the alloys after bonding. Also, phases rich in hafnium and tantalum had precipitated near the bond line in the APMT. Iron from the APMT had diffused into the superalloys during bonding, more extensively in the CM247LC than in the Rene 80. Nickel from the superalloys had diffused into the APMT, again more extensively in the joint with the CM247LC than with the Rene 80. One-inch-diameter buttons were machined from each of the bonded blocks and sent to Siemens for standard oxidation, spallation, and corrosion testing, which should be complete in the spring of 2016. A total of 16 APMT–CM247LC and 19 APMT–Rene 80 buttons were sent.

PREPARATION AND TESTING OF CORROSION- AND SPALLATION-RESISTANT COATINGS

INTRODUCTION

The objective of this Energy & Environmental Research Center (EERC) project was to take a recently developed method of plating nickel superalloys with protective FeCrAl layers closer to commercial use in syngas-fired turbines. The project is designed to determine if plating APMT®, a specific highly oxidation-resistant oxide dispersion-strengthened FeCrAl alloy made by Kanthal, onto nickel-based superalloy turbine parts is a viable method for substantially improving the lifetimes and maximum use temperatures of the parts, both those with thermal barrier coatings (TBCs) and those without. The superalloys being investigated for protection are CM247LC and Rene® 80, both alumina scale-forming alloys. The method for bonding the APMT plate to the superalloys is called evaporative metal bonding (EMB), which involves placing a thin foil of zinc between the plate and the superalloy, clamping them together, and heating in an atmosphere-controlled furnace. Upon heating, the zinc melts and dissolves the oxide skins of the alloys at the bond line, allowing the two alloys to diffuse into each other. The zinc then diffuses through the alloys and evaporates from their surfaces.

If successful, the information developed will help move the protection process closer to demonstration testing. In addition, the team will characterize the microcontaminants in combusted higher-hydrogen-content gas. This information will be used to best simulate actual corrosion conditions in a turbine system and can also be used by other researchers studying deposition and gas flow in turbines.

EXPERIMENTAL METHODS

Laboratory Testing and Modeling

Under Tasks 2 and 3, we measured properties of the alloys and developed computer models of their high-temperature properties in order to develop the best methods for joining the APMT plate to CM247LC and Rene 80 parts. In order to determine the best heating schedules to use for joining APMT plates to superalloy parts, we measured the diffusion rates of Zn through the alloys as a function of temperature. In order to develop the best clamp designs to use for holding the plating to the parts, we measured physical properties of the materials as a function of temperature. The clamp design is presented in the Results and Discussion section of this report. Once the clamp design was modeled, a clamping system was machined out of molybdenum. Under Task 5, the parts to be joined were then clamped and bonded. Cylinders or buttons of the bonded materials were then machined and sent to Siemens for standard oxidation, spallation, and corrosion testing. These tests should be completed in the spring of 2016.

RESULTS AND DISCUSSION

Laboratory Testing

Final finite element modeling has been completed to determine the clamping jig geometry for fabrication of the specimens for TBC coating and oxidation/spallation/corrosion testing. All parts of the jig are made from titanium–zirconium–molybdenum (TZM) because it has a lower coefficient of thermal expansion than the parts being bonded so those parts are put in compression upon heating of the assembly. Figure 1 shows several views of the assembly that was used to fabricate the specimens. Figure 1a is an isometric view, while Figures 1b and 1c are side and end views, respectively. Figure 1c also shows each piece of the assembly labeled with the material type.

The base metal plates of CM247LC and Rene 80 provided by Siemens are nominally 0.0256 m × 0.128 m × 0.218 m (1 in. × 5 in. × 8.5 in.). The samples were fabricated in blocks 0.128 m × 0.0513 m (5 in. × 2 in.) using the jig geometry shown in Figure 1. Three blocks were bonded for each base metal type along with one backing plate (grooved to allow the release of Zn vapor during the bonding process). The test samples machined from the joined parts are nominally 0.0254-m-diameter cylinders.

For the finite element modeling, all materials in the assembly in Figure 1 were assumed to remain elastic except for the E52100 steel. A temperature-dependent, bilinear, isotropic hardening law was implemented for the plastic deformation of the steel based on Simsir and others (1). The Young's modulus of the steel was also assumed to be temperature-dependent according to data from Shi and Liu (2). All other material properties were assumed to be temperature-independent with the exception of the linear coefficient of thermal expansion which was measured previously in this project and reported in Braband and in Tatsinkou-Nguelo (3, 4).

Figure 2 shows an image of the grooved backing plate that is used to hold the APMT to the base metal. The backing plate is fabricated from the same material as the base metal. The surface of the backing plate is grooved to allow zinc that has diffused through the APMT layer to reach vacuum and vaporize. To prevent the backing plate from bonding to the top of the APMT, the backing plate was heated to approximately 1000°C for 1 week in air prior to diffusion bonding. Previous tests have shown that the resulting oxidation layer is sufficient to prevent diffusion bonding at the APMT–backing plate interface.

Figure 3 shows the predicted normal stresses at the interface between the APMT and the base metal at 1200°C for both base metal types. Stresses are given in Pascals, with negative values signifying compression and positive values signifying tension. With the exception of, at most, 6 mm at the outer edge, the entire surface is predicted to remain under compressive loading throughout the bonding process. Also, it is clear that the presence of the grooves on the face of the backing plate does not produce a nonuniform normal stress distribution on the bonding face. It should be noted that the compressive stresses on this face are expected to be artificially low, again due to the "bonded" condition between the backing plate and the APMT. Essentially, the APMT wants to expand more in the plane than the backing plate attached to it will allow, creating a

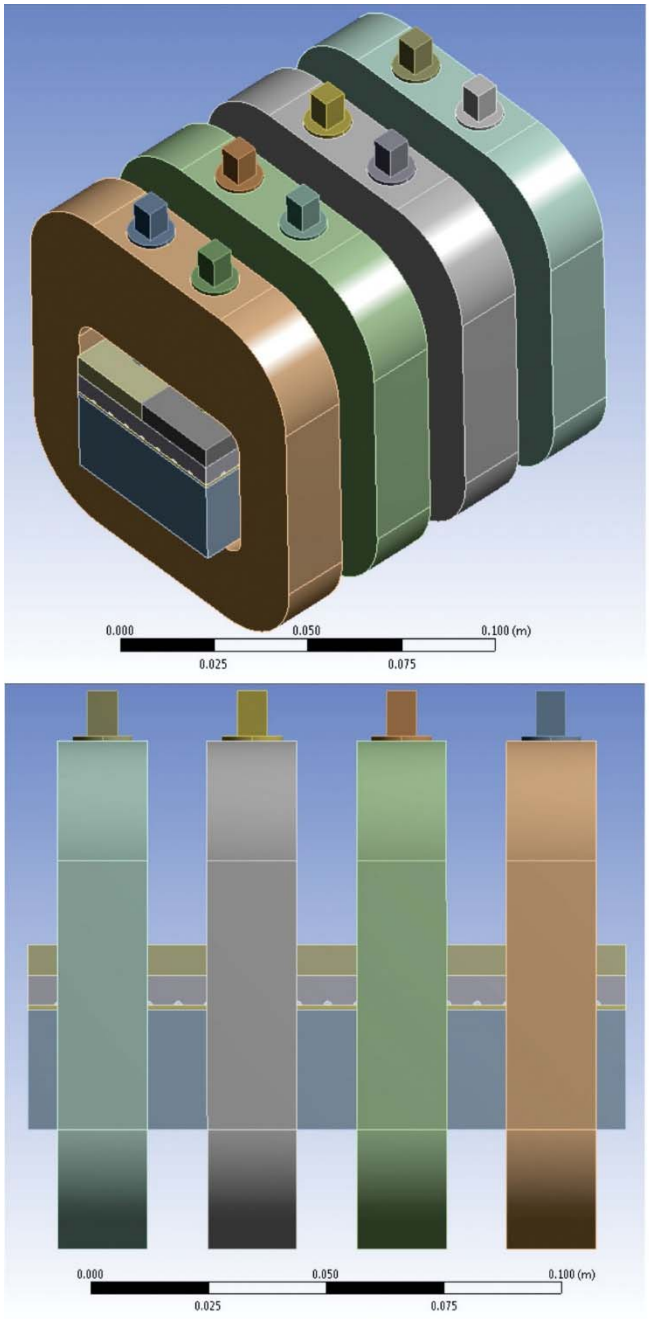

Figure 1. Jig assembly used for fabrication of the test samples (continued. . .).

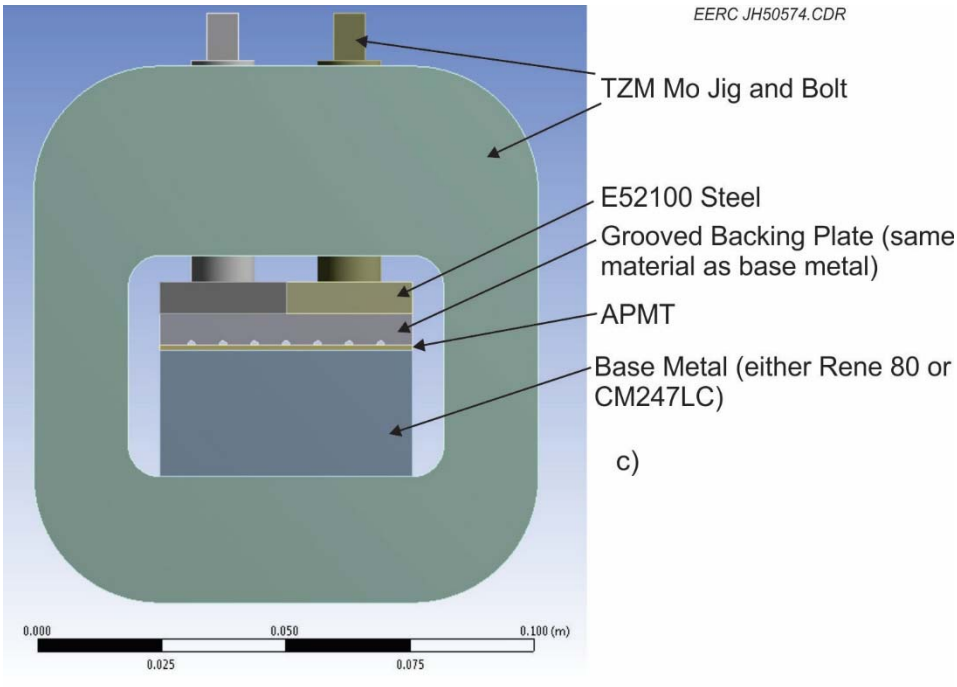

Figure 1 (continued). Jig assembly used for fabrication of the test samples.

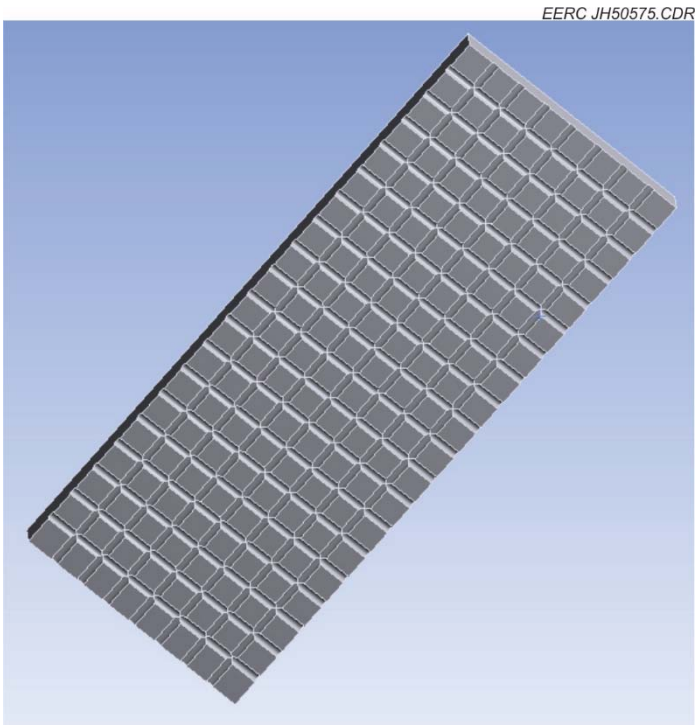

Figure 2. Grooved backing plate used to clamp the APMT to the base metal layer while allowing Zn to vaporize after reaching the top of the APMT layer.

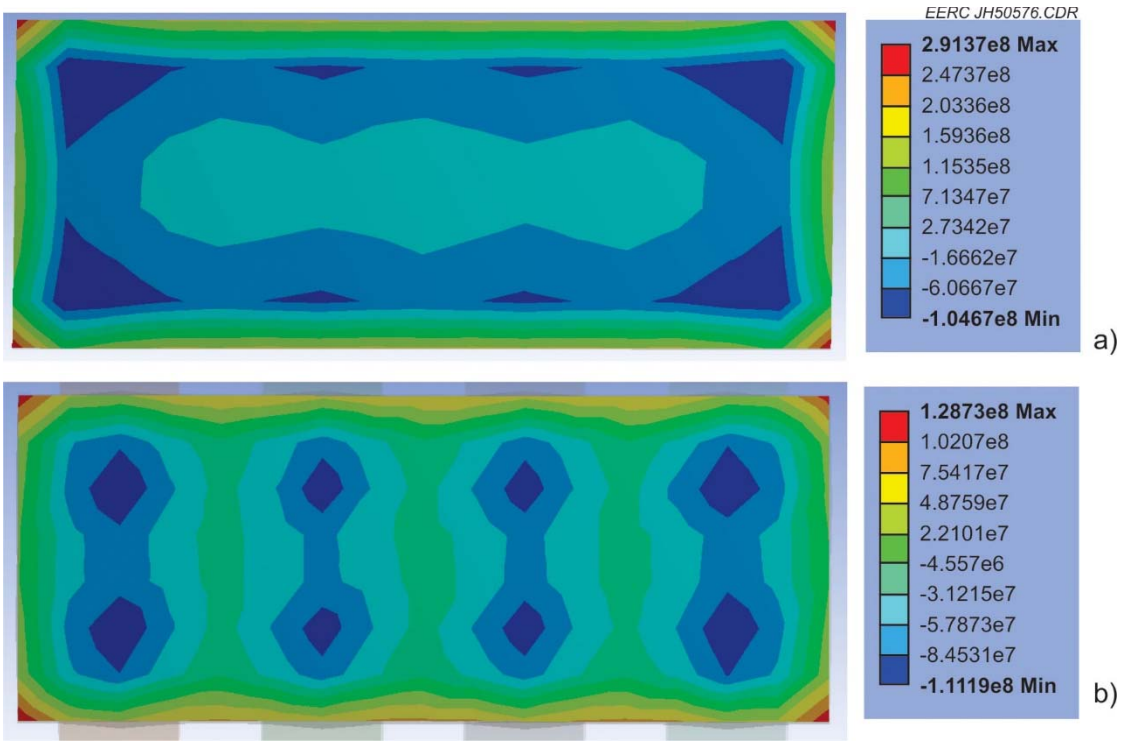

Figure 3. APMT–base metal interface normal stresses for a) CM247LC and b) Rene 80 at 1200°C.

tendency for the APMT to bow upward toward the backing plate, reducing the calculated compressive stress on this surface. The stresses within the plane of the APMT caused by this boundary condition are shown in Figure 4. In practice, this effect should be much lower, as the APMT will not be prevented from expanding except by friction.

Figure 5 shows the predicted equivalent (von Mises) stresses in the TZM jig. Figure 6 shows the normal stresses acting on the lower interior face of the jig as well. While Figure 5 seems to predict unacceptably high stresses in the lower region of the jig, comparison with Figure 6 shows that the normal stresses in this region are quite low. Thus the elevated equivalent stresses are arising because of the interface condition chosen for the finite element modeling. To achieve convergence at all temperatures, all interfaces had to be set to "bonded." In practice, lateral motion of adjacent surfaces due to difference in thermal expansion, for example, is possible. In the model, it is not. This additional constraint produces artificially high equivalent stresses in the lower region of the joint that will not actually occur during fabrication.

Similarly, Figure 7 shows the equivalent (von Mises) stresses in the TZM Mo bolts. The very high values of stress at the base of the bolts arise because of the artificial "bonded" constraint at the interface with the steel plate. The difference in thermal expansion as well as the plastic deformation of the steel should cause significant sliding at the interface that is not allowed in the finite element model.

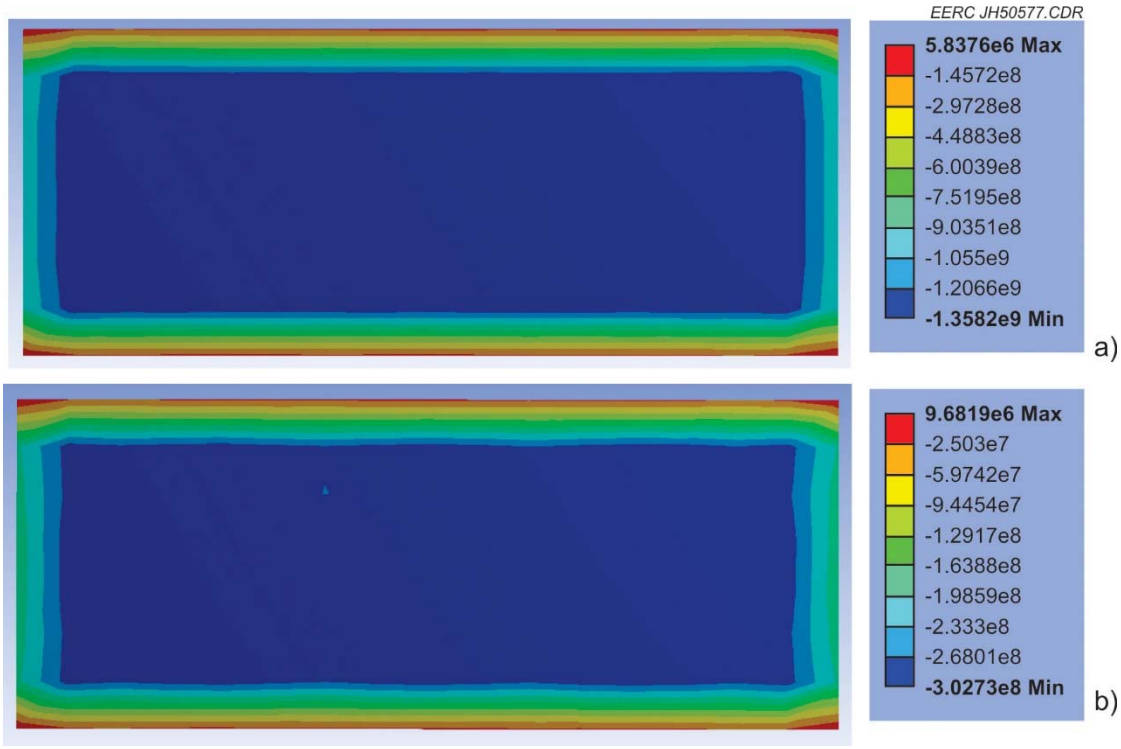

Figure 4. Normal stresses in the plane of the APMT for a) CM247LC and b) Rene 80 at 1200°C.

Based on the finite element results, the jig assembly shown in Figure 1 should be able to successfully fabricate the samples for further oxidation/spallation/corrosion testing. Moreover, the general approach to designing jigs for larger/more complicated assemblies (i.e., a series of narrow jigs relatively closely spaced rather than a single continuous clamping plate) seems to be able to maintain the requisite bonding stresses while minimizing the jig material needed and the complexity of jig manufacturing.

After the modeling of the clamping system was completed, the jig parts were machined from blocks of TZM molybdenum. Figure 8 shows the individual pieces. Figure 9 shows the pieces as assembled in preparation for heating to bond the APMT plate to the surface of the nickel superalloys.

After the first blocks of each superalloy were bonded, two 5-mm-thick sections were cut from one end of each of the bonded blocks using electrical discharge machining and polished for analysis in a FEI Quanta™ FEG 650 series scanning electron microscope. The preliminary analyses were done to make sure that the bonds were complete, to determine whether or not the zinc had completely evaporated from the APMT and superalloys, and to determine what sort of interactions occurred between the APMT and superalloys.

The SEM analyses were done at magnifications from 100× to 1000×, and the accelerating voltage of the electron beam was between 5 and 15 kV. The bond lines between the superalloys

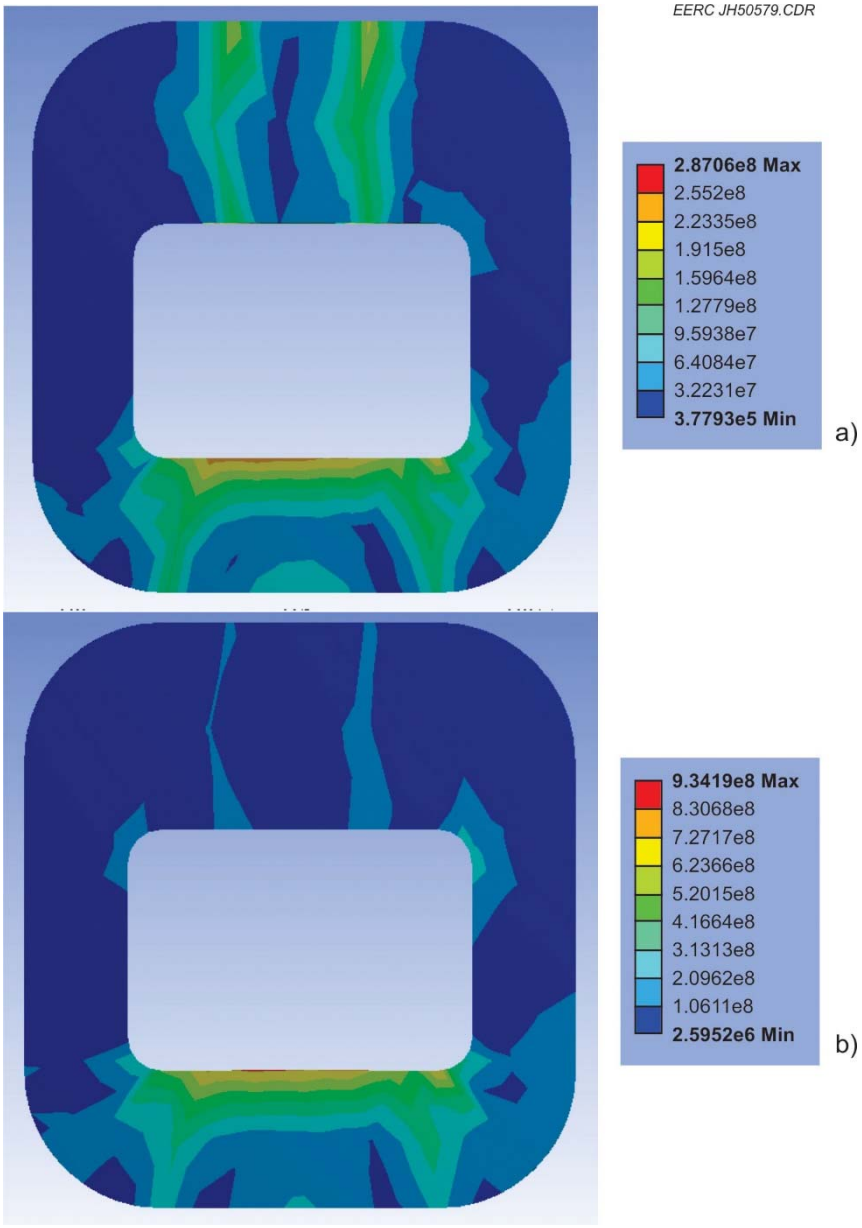

Figure 5. TZM Mo jig equivalent (von Mises) stresses for a) CM247LC and b) Rene 80 at 1200°C.

(bottom) and the APMT (top) are shown in Figures 10 and 11. They show that new phases have precipitated near the bond lines in both metals because of elemental diffusion between the parts. The precipitates will be further investigated in future analyses, but in previous work it was found that the strength of the joints with CM247LC were greater than that of the APMT. Rene 80 had not been previously tested. No zinc was detected in any analyses, indicating that if it is present, its concentration is below 0.1 weight percent.

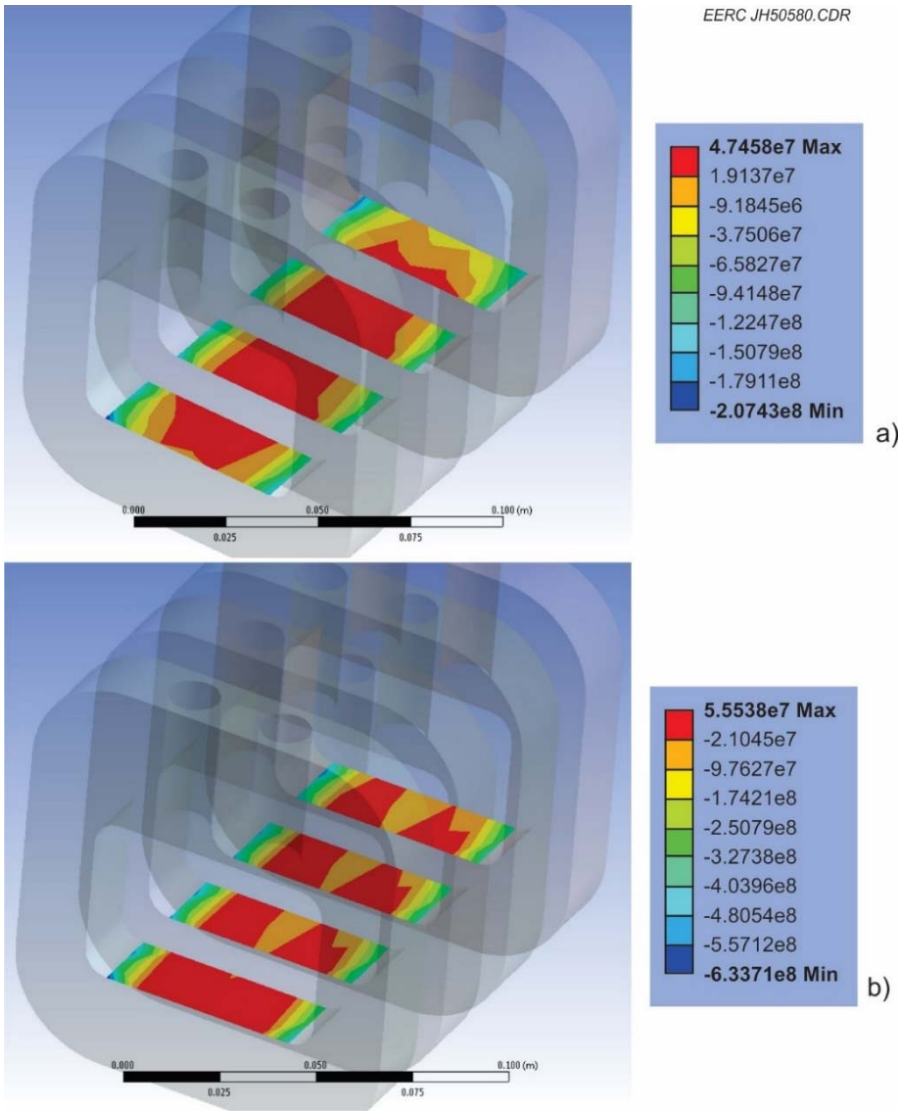

Figure 6. Base metal–TZM Mo jig normal stresses for a) CM247LC and b) Rene 80 at 1200°C.

After determining that no zinc remained in the alloys being joined, the remaining blocks were bonded. It was found that one bond for each superalloy was weak, possibly because the superalloy oxidized at room temperature enough to prevent the bonding since they were sandblasted approximately 1 month before bonding. The other bonded pieces were sandblasted the day before bonding and appear to have strong bonds.

One-inch-diameter cylindrical buttons were electrodischarge-machined (EDM) from each of the bonded blocks. A total of 16 CM247LC buttons and 19 Rene 80 buttons were prepared and shipped to Siemens, which has performed precipitation hardening of the superalloys. They will then be covered with a thermal barrier coating on the APMT, and Siemens will perform standard oxidation, spallation, and corrosion testing of the buttons. By performing the same tests that they have already done on the APMT and the two superalloys, we will be able to directly compare those results to the results for the APMT–superalloy bonded parts.

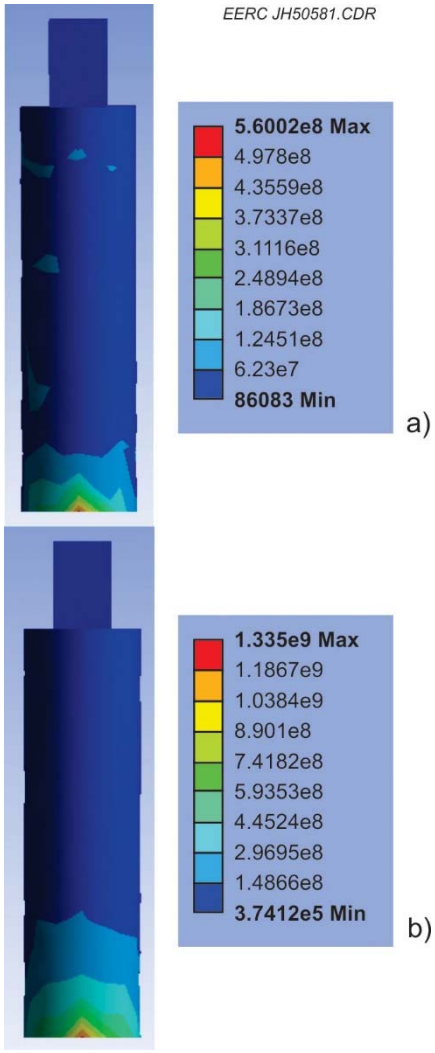

Figure 7. Base metal–TZM Mo jig normal stresses for a) CM247LC and b) Rene 80 at 1200°C.

In order to determine the morphologies of the diffusion-affected zones in the bond areas, pieces of the plates remaining after EDM were polished for analyses in a FEI Quanta FEG 650 series scanning electron microscopy. The electron beam accelerating voltage was 15 kV. A circular backscatter detector was used for imaging. Energy dispersive x-ray spectroscopy was used to determine the compositions of the different phases.

It should be noted that these bonded pieces have not been precipitation-hardened. In the next quarter, we will analyze bonded pieces that have been put through the precipitation-hardening step.

Figure 8. The clamping jig and parts to be bonded.

Figure 9. The assembled jig in preparation for heating to bond the APMT plate to the superalloy block.

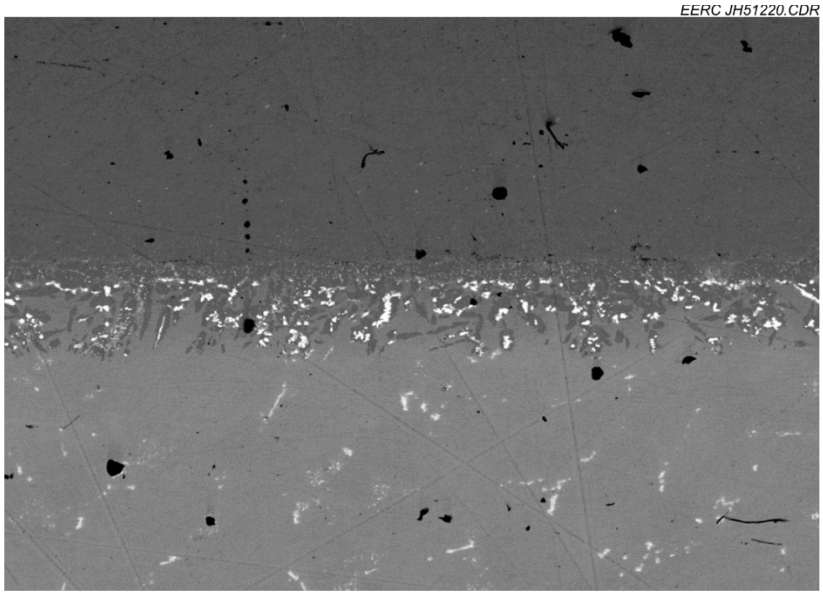

Figure 10. Bond line between CM247LC (bottom) and APMT (top) at 100× magnification.

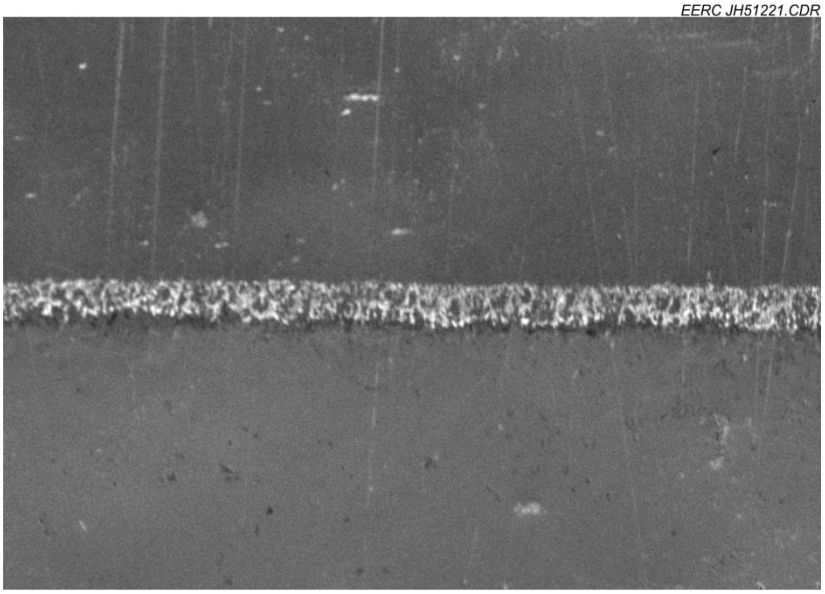

Figure 11. Bond line between Rene 80 (bottom) and APMT (top) at 100× magnification.

For comparison purposes to the SEM data, the compositions of the base alloys are given in Table 1. Figure 12 shows the bond line or joint between the APMT plate (top) and the CM247LC (bottom). The compositions of the precipitates or areas labeled in the following SEM images are given in the tables following each figure. The compositions given in the SEM composition tables are averages from the spot analyses of five different grains for each precipitate or area type labeled.

As the composition data for Figure 12 show, no Zn remains at the bond line (joint). The bright precipitates are Hf- and Ta-rich, whereas the dark precipitates are rich in Al oxide. Figure 13 shows precipitates within the APMT near a CM247LC–APMT joint. The composition data show that the bright precipitates are also Hf- and Ta-rich, whereas the darker ones contain Fe, Ni, and Al, demonstrating that Ni from the CM247LC has diffused into the APMT. Figure 14 shows a lower-magnification view of the joint between the APMT and CM247LC. The compositions of the regions within the APMT near the joint also demonstrate Ni diffusion into the APMT, whereas the compositions of regions in the CM247LC show that iron from the APMT has diffused into the superalloy.

Figure 15 shows a joint between APMT and Rene 80. There are far fewer bright precipitates near this joint because Rene 80 does not contain Hf or Ta. The dark areas are aluminum oxide-rich, and there is much less iron diffusion into the Rene 80 than there was in the CM247LC. Figure 16 shows a higher-magnification region primarily within the APMT just above the joint with the Rene 80. Here, again, the small dark particles are aluminum oxide-rich, and much less Ni has diffused into the APMT than with the CM247LC joint. Most regions within the superalloys near both joints appear depleted in Co.

CONCLUSIONS

During this year, the finite element model was completed and used to design clamping jigs to hold the APMT plate to the larger blocks of superalloys during the bonding process. The clamping system was machined from TZM and used to bond the APMT plate to the superalloy blocks. The bond between the APMT plate was weak for one of each of the superalloy blocks. We believe that this occurred because enough oxidation had occurred on the surface of the parts as a result of a 1-month time period between sandblasting to prepare the parts and the actual bonding process. The other blocks were, therefore, bonded within 1 day of preparing the parts for bonding, and their joints appear strong. SEM analyses of representative joints showed that no zinc remained in the alloys after bonding. Also, phases rich in hafnium and tantalum had precipitated near the bond line in the APMT. Iron from the APMT had diffused into the superalloys during bonding, more extensively in the CM247LC than in the Rene 80. Nickel from the superalloys had diffused into the APMT, again more extensively in the joint with the CM247LC than with the Rene 80. One-inch-diameter buttons were machined from each of the bonded blocks and sent to Siemens for standard oxidation, spallation, and corrosion testing, which should be complete in the spring of 2016.

Table 1. Compositions of the Base Metals, wt%

Composition	Fe	Ni	Cr	Al	Ti	Co	Mo	Ta	W	Nb	Hf	Mn	Si	C	W	Ti	B	Zr
AMPT	68.9		22	5			3					0.4	0.7					
CM 247 LC	–	61.4	8.1	5.6	0.7	9.5	0.5	3.2	9.5	0.1	1.4	–	–					
Rene 80	0.10	61.9	13.4	2.1		9.4	4.1			0.03				0.16	3.92	4.77	0.02	0.04

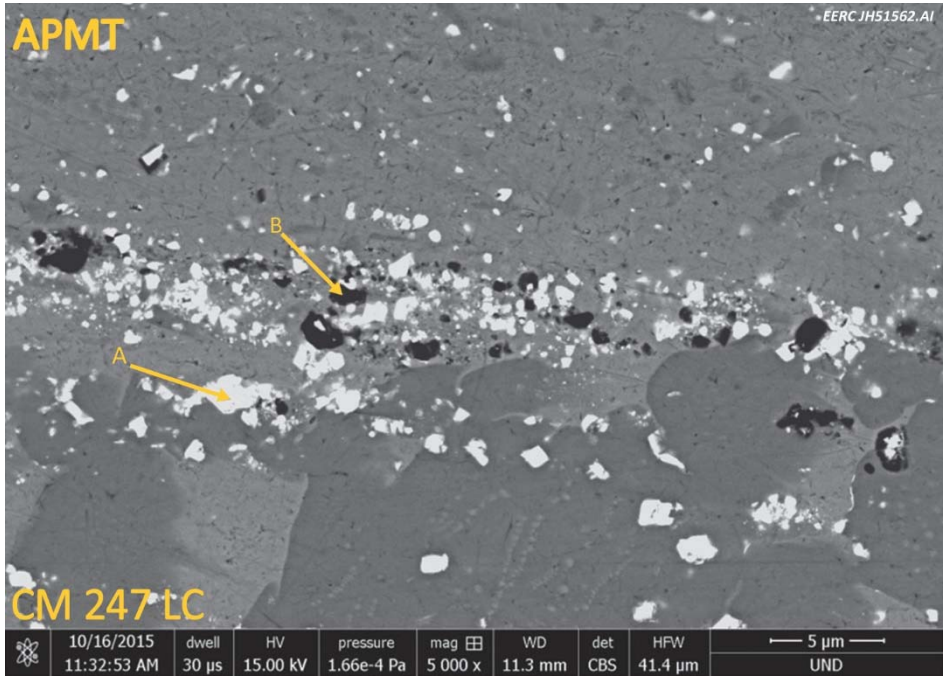

Figure 12. Precipitates at the bond line of a CM247LC–APMT joint at 5000×.

	Element, wt%												
	Fe	Ni	Cr	O	Al	Mo	Hf	Ta	Ti	Mn	Zr	Co	W
A: Small white specks found along bond line	7.1	12.8	4.9	0.0	2.7	0.0	27.8	25.0	4.3	0.0	0.0	2.2	13.2
B: Black specks found along bond line	6.6	8.2	2.9	38.8	32.6	0.8	7.2	0.0	1.0	0.0	0.0	1.9	0.0

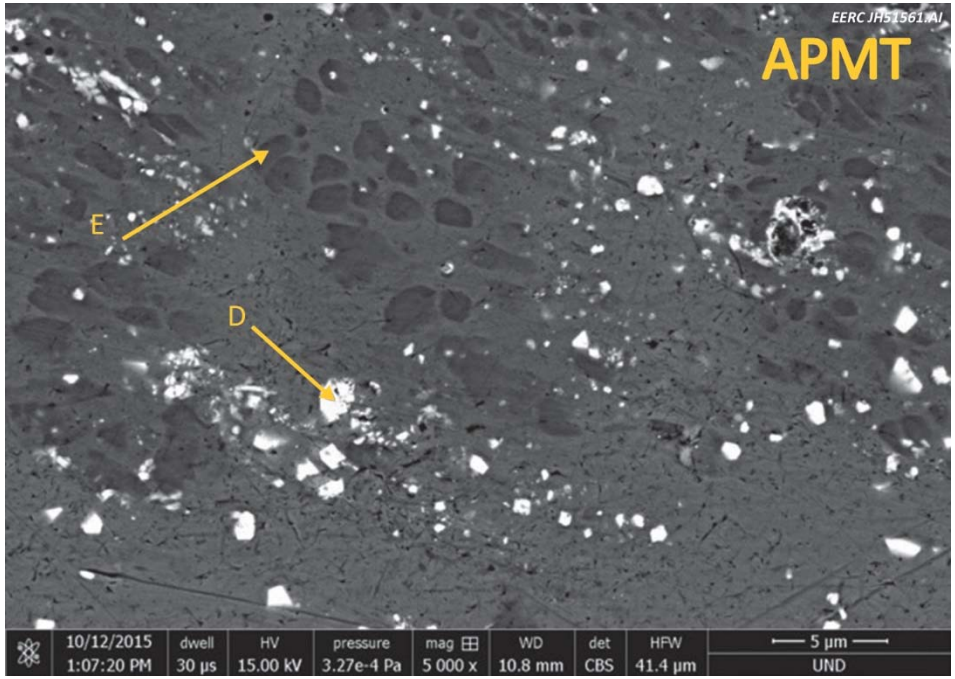

Figure 13. Precipitates within the APMT near a CM247LC–APMT joint at 5000×.

	Element, wt%												
	Fe	**Ni**	**Cr**	**O**	**Al**	**Mo**	**Hf**	**Ta**	**Ti**	**Mn**	**Zr**	**Co**	**W**
D: Small, white precipitates in APMT	8.3	3.3	3.0	0.0	0.6	0.2	23.8	42.8	14.5	0.1	2.7	0.7	0.0
E: Dark gray, small, and circular in APMT; present in APMT past 15 µm	22.7	49.5	6.5	0.0	13.4	0.3	1.0	2.8	0.2	0.2	0.0	3.4	0.0

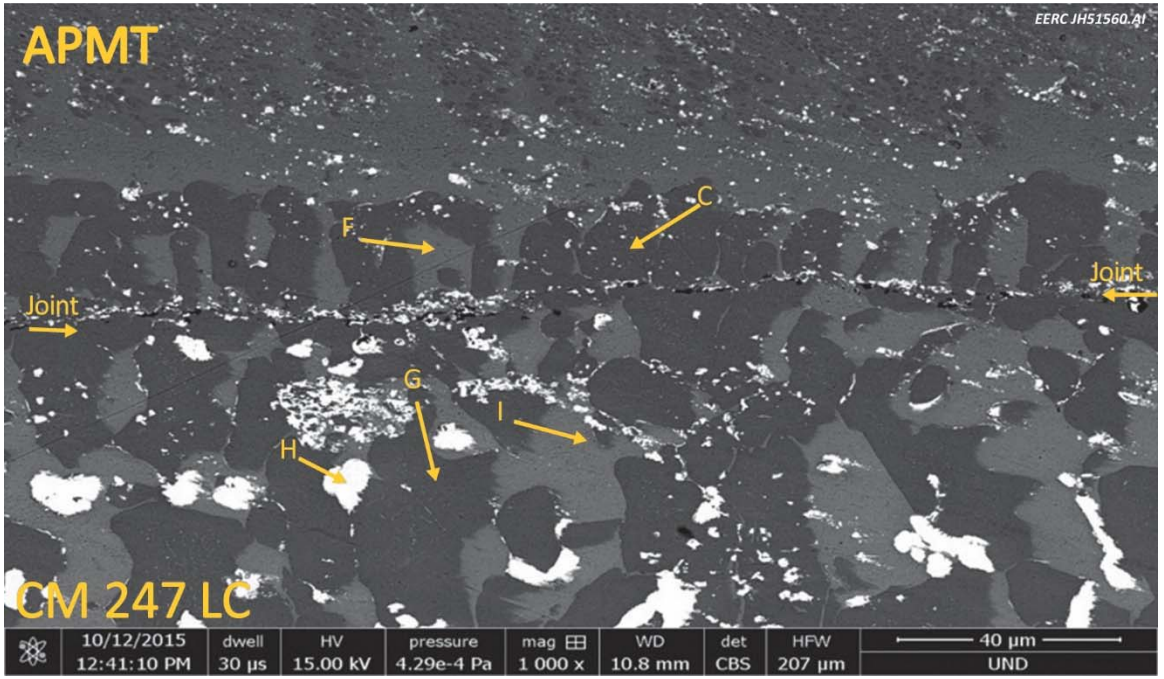

Figure 14. Larger regions of varying morphologies and compositions in the APMT (top) and the CM247LC (bottom) near the bond line (joint) at 1000×.

	Element, wt%												
	Fe	**Ni**	**Cr**	**O**	**Al**	**Mo**	**Hf**	**Ta**	**Ti**	**Mn**	**Zr**	**Co**	**W**
C: Large, dark gray areas in APMT; diffuses from 0 to 30 µm into APMT	18.8	57.8	4.4	0.0	14.2	0.0	0.0	0.0	0.0	0.0	0.0	4.8	0.0
F: Large, light gray regions in APMT; present from 0 to 40 µm	41.2	29.1	13.7	0.0	2.6	1.1	1.0	1.5	0.0	0.0	0.0	5.3	4.5
G: Large, dark gray regions in CM247LC; present from 0 to 225 µm into CM247LC	15.1	58.7	2.8	0.0	12.8	0.0	1.8	3.1	0.4	0.3	0.0	5.0	0.0
H: Large, amorphous white regions in CM247LC; present from 40 to 260 µm	14.5	7.0	8.8	0.0	0.9	2.6	3.5	57.0	0.7	0.7	0.0	4.3	0.0
I: Large, light gray regions between precipitates in CM247LC	31.5	34.8	13.5	0.0	3.4	1.5	2.5	3.6	0.9	0.8	0.0	7.5	0.0

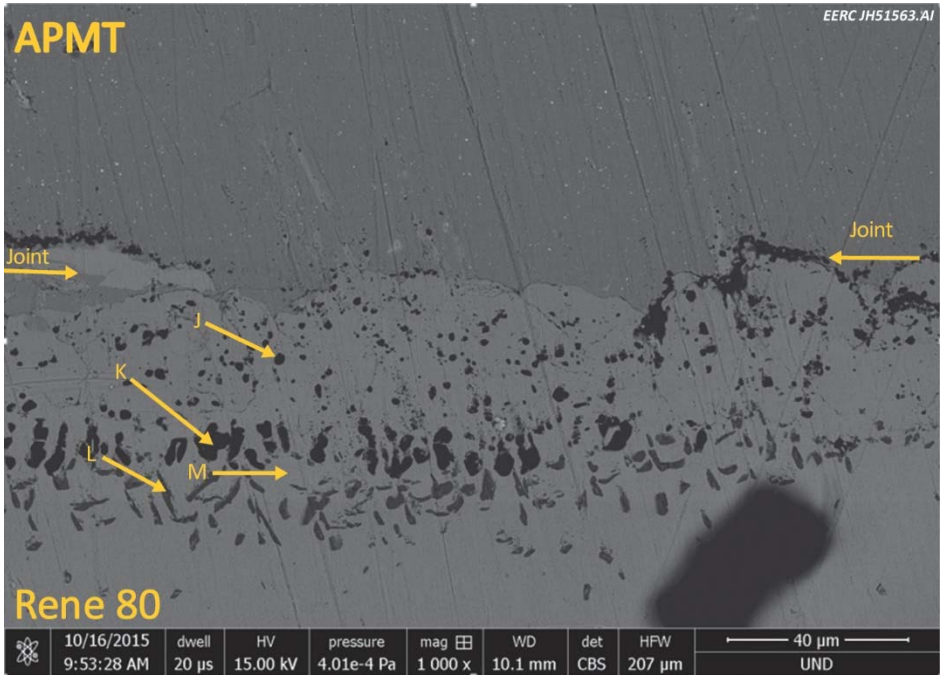

Figure 15. Morphologies near the bond line in an APMT–Rene 80 joint at 1000×.

	Element, wt%												
	Fe	**Ni**	**Cr**	**O**	**C**	**Al**	**Mo**	**Ti**	**Co**	**W**	**Zr**	**Y**	**Si**
J: Black and round precipitates in bond line; diffused up to 30 µm into base metal	2.7	12.3	4.0	37.9	6.1	33.6	0.0	0.8	2.6	0.0	0.0	0.0	0.0
K: Black precipitates in Rene 80; formed approx. 30–45 µm below bond line	0.0	2.0	0.7	47.0	3.1	47.2	0.0	0.0	0.0	0.0	0.0	0.0	0.0
L: Light gray, skinny, and long precipitates in Rene 80; formed approx. 45–60 µm below bond line	0.0	2.3	0.0	0.0	4.1	0.0	0.0	93.6	0.0	0.0	0.0	0.0	0.0
M: Gray regions in between other precipitates	3.7	64.0	8.9	0.0	3.8	3.4	3.2	3.4	9.6	0.0	0.0	0.0	0.0

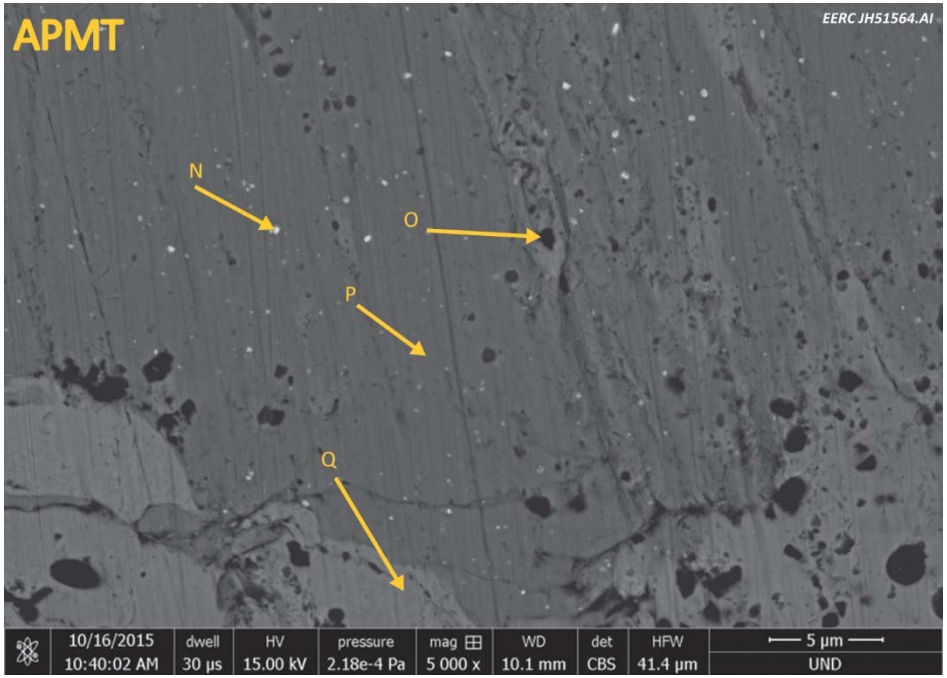

Figure 16. Precipitates in the APMT near an APMT–Rene 80 joint at 5000×.

	Element, wt%												
	Fe	**Ni**	**Cr**	**O**	**C**	**Al**	**Mo**	**Ti**	**Co**	**W**	**Zr**	**Y**	**Si**
N: White specks in APMT	50.7	3.6	11.4	0.8	13.0	2.5	0.0	2.0	0.0	0.0	7.7	0.0	8.3
O: Black specks in APMT; formed randomly and sparingly from 0 to 30 µm	44.4	2.7	10.6	15.0	5.7	12.6	1.3	0.0	0.0	0.0	0.0	7.7	0.0
P: Gray region in APMT	68.3	3.8	15.5	0.0	5.2	4.4	2.8	0.0	0.0	0.0	0.0	0.0	0.0
Q: Gray region just below bond line	69.7	4.8	15.3	0.5	3.0	3.9	2.6	0.0	0.0	0.0	0.0	0.0	0.2

REFERENCES

1. Simsir, C.; Dalgic, M.; Liibben, T.; Irretier, A.; Wolff, M.; Zoch, H.W. The Bauschinger Effect in the Supercooled Austenite of SAE 52100 Steel. *Acta Materialia,* **2010**, *58*, 4478–4491.

2. Shi, J.; Liu, C.R. On Predicting Chip Morphology and Phase Transformation in Hard Machining. *Int. J. Adv. Man. Tech*. **2006**, *27*, 645–654.

3. Braband, J. Characterization of Evaporative Metal Bonding in Superalloys for Use in Gasified Coal Turbine Generators. M.S. Thesis, University of North Dakota, Grand Forks, ND, 2013.

4. Tatsinkou-Nguelo, S. Preparation and Analysis of Evaporatively Bonded Superalloys for Use in Hydrogen Burning Gas Turbines. M.S. Thesis, 2014.